Science of the Total Environment 922 (2024) 171220

Contents lists available at ScienceDirect

Science of the Total Environment

journal homepage: www.elsevier.com/locate/scitotenv

Evaluation of 6-PPD quinone toxicity on lung of male BALB/c mice by quantitative proteomics

Wenmiao He [a,b], Jie Chao [a], Aihua Gu [b,*], Dayong Wang [a,*]

[a] Key Laboratory of Environmental Medicine Engineering of Ministry of Education, Medical School, Southeast University, Nanjing, China
[b] School of Public Health, Nanjing Medical University, Nanjing, China

HIGHLIGHTS

- Repeated 6-PPDQ injection induced inflammation and fibrosis, and impaired lung function.
- Changes of Ripk1, Fadd, Il6st, and Il16 expressions were related to 6-PPDQ-induced inflammation.
- Alteration in Smad2 expression was associated with fibrosis caused by 6-PPDQ.

GRAPHICAL ABSTRACT

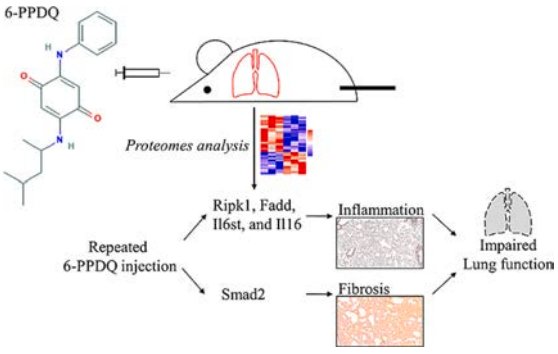

ARTICLE INFO

Editor: Henner Hollert

Keywords:
6-PPDQ
Mouse
Inflammation
Fibrosis
Lung proteomes

ABSTRACT

N-(1,3-dimethylbutyl)-*N*′-phenyl-*p*-phenylenediamine quinone (6-PPDQ), a transformation product of tyre-derived 6-PPD, has been frequently detected in different environments. After 6-PPDQ exposure, we here aimed to examine dynamic lung bioaccumulation, lung injury, and the underlying molecular basis in male BALB/c mice. After single injection at concentration of 4 mg/kg, 6-PPDQ remained in lung up to day 28, and higher level of 6-PPDQ bioaccumulation in lung was observed after repeated injection. Severe inflammation was observed in lung after both single and repeated 6-PPDQ injection as indicated by changes of inflammatory cytokines (TNF-α, IL-6 and IL-10). Sirius red staining and hydroxyproline content analysis indicated that repeated rather than single 6-PPDQ injection induced fibrosis in lung. Repeated 6-PPDQ injection also severely impaired lung function in mice by influencing chord compliance (Cchord) and enhanced pause (Penh). Proteomes analysis was further carried out to identify molecular targets of 6-PPDQ after repeated injection, which was confirmed by transcriptional expression analysis and immunohistochemistry staining. Alterations in Ripk1, Fadd, Il-6st, and Il-16 expressions were identified to be associated with inflammation induction of lung after repeated 6-PPDQ injection. Alteration in Smad2 expression was identified to be associated with fibrosis formation in lung of 6-PPDQ exposed mice. Therefore, long-term and repeated 6-PPDQ exposure potentially resulted in inflammation and fibrosis in lung by affecting certain molecular signals in mammals. Our results suggested several aspects of

* Corresponding authors.
E-mail addresses: aihuagu@njmu.edu.cn (A. Gu), dayongw@seu.edu.cn (D. Wang).

https://doi.org/10.1016/j.scitotenv.2024.171220
Received 24 October 2023; Received in revised form 28 January 2024; Accepted 21 February 2024
Available online 25 February 2024

lung injury caused by 6-PPDQ and provide the underlying molecular basis. These observations implied the possible risks of long-term 6-PPDQ exposure to human health.

1. Introduction

Tyre and road wear particles (TRWP) have drawn increasing attention due to the mass release into environment (Liu et al., 2022). Among TRWP components, *N*-(1.3-dimethylbutyl)-*N*′-phenyl-*p*-phenylenediamine quinone (6-PPDQ), the tire-derived ozonation production, could be detected in roadway runoff in USA (Tian et al., 2021). Meanwhile, 6-PPDQ was observed to be also widely distributed in other environment medias, including dust and air (Deng et al., 2022; Zhang et al., 2022). 6-PPDQ was identified in over 80 % of $PM_{2.5}$ samples collected from six megacities, and 6-PPDQ daily intakes for human was estimated at ng to μg level (Zhang et al., 2022). Some reports confirmed the 6-PPDQ occurrence in daily food and human urea, which posed the potential risks to human health (Du et al., 2022; Ji et al., 2022b). Ozonation transformation assay verified that 6-PPD could be transformed into 38 of products, and 6-PPDQ was one of the most prominent products (Seiwert et al., 2022). 6-PPDQ level in wastewater changed along with weather, notably, snow significantly increased its concentration (Seiwert et al., 2022).

6-PPDQ presented high toxicity to multiple commercial fishes, especially for salmonid species (Hiki and Yamamoto, 2022). In the aquatic model animal *Danio rerio*, 6-PPDQ exposure induced obvious neurotoxicity, as characterized by abnormal body posture (Ji et al., 2022a). Interestingly, 6-PPDQ and its former 6-PPD showed obviously different transcription profiling and target tissues in *Danio rerio*, and 6-PPDQ exhibited intestinal toxicity, as shown by enlarged intestine and blood-coagulated gut (Zhang et al., 2023). In *Caenorhabditis elegans*, 6-PPDQ exposure caused intestinal toxicity, reproductive toxicity, neurotoxicity, altered lipid and dopamine metabolisms, and reduction in lifepan and healthspan (Hua et al., 2023a, 2023b, 2023c; Hua and Wang, 2023a; Hua and Wang, 2023b; Wang et al., 2023a). These observations have suggested the ecological risk of 6-PPDQ exposure.

As for the 6-PPDQ toxicity to mammalians, it was observed that 6-PPDQ oral administration caused damage on liver tissue of mice, as verified by activated inflammation and disturbed glycolipid metabolism (Fang et al., 2023). After intraperitoneal injection, the systemic toxicity evaluation of 6-PPDQ in mice suggested that 6-PPDQ was mainly accumulated in liver, lung, and kidney after 4-week injection at 4 mg/kg bw, and induced severe pathological changes in multiple organs, including both liver and lung (He et al., 2023).

The lung is the organ that performs gas exchange with large area of capillaries, around 126 m^2 in adult man (Suresh and Shimoda, 2016). Environmental pollutants or microorganisms, such as silicon dioxide and respiratory viruses, can enter the lung after breaking through the trachea (Islam et al., 2021), and act on the lung due to its large surface area (Foth, 1995). Slight injury in lung is healed by normal physiological repair, but excessive and sustained stress can trigger fibrosis process in the damaged part, leading to impairment of lung function (Borthwick et al., 2013). Recently, we observed that exposure to 6-PPDQ could cause severe pathological changes in lung of mice as characterized by swollen alveolar capillaries and exudation (He et al., 2023). However, the underlying mechanism for this lung injury remains largely unclear.

Thus, the main aim of this study was to determine underlying mechanisms of 6-PPDQ-induced lung injury using proteomics technique. Single and repeated intraperitoneal 6-PPDQ injections were performed to compare the different effects. Our data demonstrated that 6-PPDQ still remained in lung tissue 28 days after single injection, and high level of 6-PPDQ was detected in lung after repeated injection. Importantly, both single and repeated injection induced inflammation in lung, while repeated injection induced fibrosis in lung, and severely impaired lung function. The proteomes analysis further provided important molecular basis for the observed inflammation and fibrosis caused by 6-PPDQ exposure in mice.

2. Materials and methods

2.1. Animal and 6-PPDQ exposure

Male BALB/c mice (6–8 weeks old) were purchased from Gempharmatech Co., Ltd. (Nanjing, China). 6-PPDQ (97 % of purity, Toronto Research Chemicals, Toronto, Canada) was dissolved in olive oil as our previously described (He et al., 2023).

Our previous study has shown that intraperitoneal injection with 6-PPDQ could cause injury on multiple organs, including the lung (He et al., 2023). Intraperitoneal injection is of high bioavailability, and 6-PPDQ via intraperitoneal injection can be quickly absorbed into the systemic circulation, which is more helpful to determine the toxicity of 6-PPDQ. Thus, the intraperitoneal injection of 6-PPDQ was further performed in this study. Two series of animal experiments were performed. In the first series of animal experiment, mice were treated with single 6-PPDQ injection to evaluate the 6-PPDQ residual along time in lung tissue. Thirty-six mice were divided into two groups, control group and single injection group. The mice in single injection group were treated with intraperitoneal injection of 400 μL of 0.25 mg/mL 6-PPDQ (4 mg/kg bw) at day 0, and the concentration of 6-PPDQ was selected based on our previous observation (He et al., 2023). At the same time, mice in control group were injected with olive oil at the same volume. Subsequently, the lung was collected at 1, 2, 4, 7, 14, or 28 day post injection for 6-PPDQ detection for control group and single injection group, and three biological replicates were performed at each time point. In the second series of animal experiment, mice were treated with repeated 6-PPDQ injection to evaluate the lung injury. Eighteen mice were divided into three groups, control group and repeated injection groups of low and high doses (0.4 and 4 mg/kg bw), and the 6-PPDQ concentrations were selected as described previously (He et al., 2023). Exposure groups were injected intraperitoneally with 6-PPDQ every 4 days for 4 weeks (7 times), and control group was treated with olive oil at the same volume and times. At day 29, lung functions of mice were measured. After that, mice were sacrifice for lung collection. Animal experimental protocols were approved by Southeast University Faculty of Medicine Animal Experimental Committee.

2.2. 6-PPDQ concentration measurement by HPLC-MS/MS

6-PPDQ concentration in lung and serum was measured by high performance liquid chromatography coupled to a tandem mass spectrometer (HPLC-MS/MS). As for lung tissue, approximately 100 mg of lung tissue was separated, and homogenized twice in acetonitrile. Then, the total supernatant was collected into clean-up tubes (Waters, USA), and vortexed to remove impurities. Supernatant was concentrated, dissolved in 500 μL acetonitrile, and filtered with 0.22 μm filter. As for serum, 100 μL of serum was mixed with acetonitrile, homogenized twice, and then the supernatant was cleaned and concentrated as described above. 6-PPDQ measurement was performed in Ultimate 3000/Q Exactive (UHPLC-Q-Obitrap MS, Thermo Scientific, USA). The detailed parameters were the same as our previous study (He et al., 2023). Three or six independent samples were tested for each group.

2.3. Sirius red staining

Sirius red staining was used to assess fibrosis in lung (Borthwick et al., 2013). Upon sacrifice, mouse lung was isolated. Part of lung tissue

was fixed in 4 % formaldehyde. The lung tissue was dehydrated, cleared, and embedded in paraffin. Tissues were cut into sections of 5 μm thickness, and stained with Weigert's hematoxylin and Sirius red (Solarbio, Beijing, China). The collagen in tissue can be marked in red by Sirius red dye. Quantification of collagen area in sections was performed by Image J software. Experiments were repeated three times.

2.4. Immunohistochemistry analysis

Immunohistochemical analysis was applied to evaluate distribution and level of proteins in lung tissue. First, antigen repair was conducted at 100 °C with citrate buffer solution. Then, sections were incubated with primary antibody (TNF-α (Cat: GB11188), Servicebio, China; p-Ripk1 (Cat: 38662S), CST, USA; Ripk1 (Cat: 17519-1-AP), Proteintech, China; p-Smad2 (Cat: PA5-105000), Thermo Fisher, USA; Smad2 (Cat: EM1701-44), HUABIO, China) and horseradish peroxidase-labeled secondary antibody. The positive area of protein in sections was quantified with Image J software. Experiments were repeated three times.

2.5. ELISA assay of inflammatory cytokines and hydroxyproline content analysis

Levels of inflammatory cytokines (TNF-α, IL-6, and IL-10) in lung tissue and serum were also measured by mouse TNF-α enzyme-linked immunosorbent assay (ELISA) kit (catalogue number: FMS-ELM00, Fcmacs Biotechnology, Nanjing, China), mouse IL-6 ELISA kit (catalogue number: FMS-ELM006, Fcmacs Biotechnology, Nanjing, China), and mouse IL-10 ELISA kit (catalogue number: FMS-ELM009, Fcmacs Biotechnology, Nanjing, China). Serum for each mouse (100 μL) was collected for ELISA. Approximate 100 mg tissue was separated and homogenized. Supernatant was collected for cytokine measurement according to the protocols. OD values were determined by Multiskan FC (Thermo Scientific, Massachusetts, USA). Cytokine levels were calculated by referring to the standard curve. Six independent samples in each group were performed.

Level of hydroxyproline in lung tissue was determined by Hydroxyproline assay (ELISA) kit (catalogue number: A030-1-1, Jiancheng Bioengineering Institute, Nanjing, China). Approximate 100 mg tissue was separated and homogenized. Supernatant was collected for cytokine measurement according to the protocols. OD values were determined by Multiskan FC (Thermo Scientific, Massachusetts, USA). Hydroxyproline content was calculated by referring to the standard curve. Six independent samples in each group were performed.

2.6. Lung function test

Mouse lung function was measured with plethysmograph system CRFM100 (EMMS, England). Mice were anesthetized by intraperitoneal injection with pentobarbital sodium (50 mg/kg). Then, neck skin was cut to expose the trachea. Intubation needle was inserted into the trachea, and needle was fixed with surgical suture. Needle in trachea was connected with instrument, and lung functions (forced expiratory volume in 50 ms (FEV50), forced vital capacity (FVC), FEV50/FVC, total lung capacity (TLC), quasi-static lung compliance, also named chord compliance (Cchord), and enhanced pause (Penh)) were tested according to the protocol. Forced expiratory volume in 50 ms (FEV50), forced vital capacity (FVC), forced expiratory volume in 50 ms/forced vital capacity (FEV50/FVC), total lung capacity (TLC), quasi-static lung compliance (Cchord), and enhanced pause (Penh) were determined at day 29 after repeated injection. Six independent samples each group were performed.

2.7. Quantitative proteomes analysis of lung tissue

Approximately 100 mg of lung tissue of repeated injection group (4 mg/kg bw) and the control group was collected for proteomics analysis, and three independent samples were collected for each group. Total proteins of lung tissue were extracted with SDT lysis buffer (Saiguo bio, Guangzhou, China), quantified by BCA protein quantification kit (catalogue number: E112-01, vazyme, Nanjing, China), and digested into pure peptides by filter-aided sample preparation (FASP) (Wiśniewski et al., 2009). Peptides from samples were separated and quantified in HPLC system nanoElute (Bruker, Germany) coupled with mass spectrometer timsTOF Pro (Bruker, Germany). MaxQuant (Germany), a proteome software, was used to identify and quantify proteins from peptide data. Based on differently expressed proteins (fold change > 2.0 or <0.5, and $p < 0.05$), Kyoto Encyclopedia of Genes and Genomes (KEGG) pathway analysis and Gene Ontology (GO) analysis were tested to perform functional analysis.

For the detailed parameters of HPLC system nanoElute coupled with mass spectrometer timsTOF Pro, the EASY C18 column (25 cm × 75 μm, 1.9 μm, Thermo Scientific, USA) was used. The used mobile phases were (A) 0.1 % formic acid in water and (B) 0.1 % formic acid in acetonitrile, and the flow rate was 300 nL/min. A capillary voltage of 1.5 kV was used in positive ionization mode, and the mass spectrum scan range was between *m/z* 100 and 1700. Parallel accumulation serial fragmentation (PASEF) method was applied for data acquisition, and the 1/K0 was 0.6–1.6 V·s/cm^2, then 10 PASEF MS/MS was performed.

2.8. Real-time PCR analysis

Real-time polymerase chain reaction (RT-PCR) assay was performed to assess transcriptional levels of targets gene in response to 6-PPDQ. Approximately 100 mg lung tissue was separated and homogenized. Trizol (Thermo Fisher, USA) was used for RNA extraction according to the protocol. RNA concentration was determined by Nanodrop one (Thermo Fisher, USA). Complementary DNA (cDNA) was synthesized with HiScript reverse transcriptase (Vazyme, China). RT-PCR was performed with AceQ qPCR SYBR Green Master Mix in LightCycler 480 (Roche, Switzerland). The relative mRNA expression was calculated by $^{\Delta\Delta}$Ct method. Three independent samples each group were performed. Sequences for primers are presented as follows: *β-actin* (forward: 5′-GTGACGTTGACATCCGTAAAGA-3′, reverse: 5′-GCCGGACTCATCGTACTCC-3′), *Ripk1* (forward: 5′-GAAGACAGACCTAGACAGCGG-3′, reverse: 5′-CCAGTAGCTTCACCACTCGAC-3′), *Fadd* (forward: 5′-GCGCCGACACGATCTACTG-3′, reverse: 5′-GCGCCGACACGATCTACTG-3′), *Il-6st* (forward: 5′-TTACTACGTGAATGCCAGCTACA-3′, reverse: 5′-GACGTGGTTCTGTTGATGACA-3′), *Il-16* (forward: 5′-AAGAGCCGGAAATCCACGAAA −3′, reverse: 5′-GTCTCAAAAGGGTCAGGGTACT-3′), and *smad2* (forward: 5′-ATGTCGTCCATCTTGCCATTC-3′, reverse: 5′-AACCGTCCTGTTTTCTTTAGCTT-3′). Among above mentioned genes, *β-actin* acts as the internal reference gene.

2.9. Statistical analyses

Data were presented as mean ± standard deviation (SD). Significance between groups was analyzed by Student's *t*-test or one-way ANOVA in SPSS software. Assumption checking and homogeneity of variance were tested before significance analysis. Probability levels of 0.05 (*) and 0.01 (**) were considered to be significant.

3. Results

3.1. 6-PPDQ dynamic bioaccumulation in lung after single and repeated injection

We performed single and repeated injection to evaluate 6-PPDQ dynamic bioaccumulation in lung by HPLC-MS/MS. After single injection of 4 mg/kg 6-PPDQ at day 0, 6-PPDQ level in lung declined sharply from 1 day to 7 days post injection (from 15.54 ± 2.21 ng/g at day 1 to 3.43 ± 0.52 ng/g at day 7) (Fig. 1A). After that, 6-PPDQ level in lung presented a gradual and slow decline 7 days post injection (from 3.43 ±

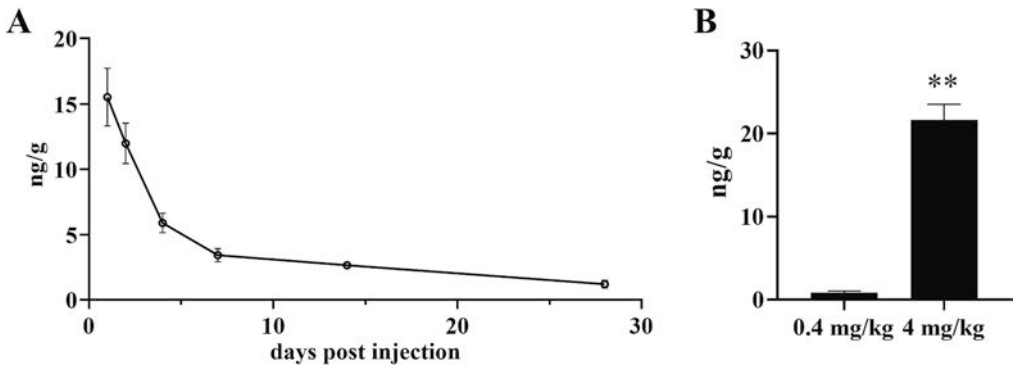

Fig. 1. 6-PPDQ dynamic bioaccumulation in lung after single and repeated injection. (A) Lung 6-PPDQ level at day 1, 2, 4, 7, 14, and 28 after single injection of 4 mg/kg 6-PPDQ at day 0. Three independent samples were tested in each group. (B) Lung 6-PPDQ level after repeated injection of 0.4 and 4 mg/kg 6-PPDQ for 4 weeks. Six independent samples were tested in each group. $^{*}P < 0.05$, $^{**}P < 0.01$.

0.52 ng/g at day 7 to 1.21 ± 0.29 ng/g at day 28) (Fig. 1A). After repeated injection of 0.4 and 4 mg/kg 6-PPDQ, 0.86 ± 0.19 ng/g and 21.67 ± 1.86 ng/g level of 6-PPDQ was detected in lung, respectively (Fig. 1B). In serum, 0.60 ± 0.19 μg/L and 2.32 ± 0.42 μg/L level of 6-PPDQ was detected after repeated injection of 0.4 and 4 mg/kg 6-PPDQ (Fig. S1A).

3.2. Inflammation in lung induced by 6-PPDQ single and repeated injection

We evaluated inflammation in lung by determination of inflammatory cytokine levels using immunohistochemistry and ELISA. TNF-α and IL-6 are pro-inflammatory cytokine, and IL-10 is anti-inflammatory cytokine. In single injected mice, 4 mg/kg 6-PPDQ significantly increased TNF-α level in lung tissue as measured by both immunohistochemistry analysis (3.50 times) and ELISA assay (1.26 times) (Fig. 2A and B). In addition, 6-PPDQ also significantly increased IL-6 (1.31 times) and IL-10 (1.49 times) level in lung tissue (Fig. 2A and B).

In repeated injected mice, immunohistochemistry analysis showed that both 0.4 and 4 mg/kg 6-PPDQ increased TNF-α level (3.47 and 8.35 times) in lung tissue (Fig. 2C and D). Meanwhile, ELISA assay showed that 0.4 and 4 mg/kg 6-PPDQ significantly upregulated TNF-α (1.38 and 1.76 times) and IL-6 (1.32 and 1.92 times) levels in lung tissue (Fig. 2C and D). Levels of TNF-α (1.28 times) and IL-6 (1.45 times) in 4 mg/kg 6-PPDQ exposed mice were higher than those in 0.4 mg/kg 6-PPDQ exposed mice (Fig. 2C and D). Level of anti-inflammatory cytokine IL-10 (1.77 times) was increased by 0.4 mg/kg 6-PPDQ exposed mice (Fig. 2D). The IL-10 level (0.71 times) in 4 mg/kg 6-PPDQ injected mice was lower than that of 0.4 mg/kg 6-PPDQ injected mice (Fig. 2D).

Meanwhile, pro-inflammatory cytokines (TNF-α and IL-6) and anti-inflammatory cytokines (IL-10) in serum were determined using ELISA. In single injected mice, 4 mg/kg 6-PPDQ significantly increased TNF-α (1.36 times), IL-6 (1.41 times) and IL-10 (1.89 times) in serum (Fig. S1B). In repeated injected mice, 0.4 and 4 mg/kg 6-PPDQ significantly upregulated TNF-α (1.57 and 2.59 times), and IL-6 (1.38 and 2.24 times) in serum (Fig. S1C). Level of serum IL-10 (1.83 times) was increased by 0.4 mg/kg 6-PPDQ compared to control. The serum IL-10 level (0.56 times) in 4 mg/kg 6-PPDQ injected mice was lower than that of 0.4 mg/kg 6-PPDQ injected mice (Fig. S1C).

3.3. Fibrosis in lung induced by 6-PPDQ repeated injection

Considering that chronic inflammation can result in tissue fibrosis (Borthwick et al., 2013), fibrosis level in lung was further determined. Based on Sirius red staining in lung sections, single injection of 4 mg/kg 6-PPDQ did not change the collagen content compared to control (Fig. 3A). Different from this, repeated injection with 0.4 and 4 mg/kg 6-PPDQ significantly increased the collagen content (2.53 and 4.51 times) (Fig. 3C). As for another fibrosis maker, hydroxyproline content was not changed by single injection of 4 mg/kg 6-PPDQ (Fig. 3B), but significantly upregulated (1.43 and 1.98 times) by repeated injection of 0.4 and 4 mg/kg 6-PPDQ (Fig. 3D). These observations suggested that repeated rather than single injection of 6-PPDQ induced the lung fibrosis.

3.4. Repeated 6-PPDQ injection impaired lung function

Because both inflammation and fibrosis happened in lung of repeated injection groups, lung functions were further monitored after repeated exposure. The results showed that FEV50, FVC, FEV50/FVC, and TLC were not changed by repeated injection with 0.4 and 4 mg/kg 6-PPDQ (Fig. 4). Nevertheless, Cchord (0.92 and 0.86 times) and Penh (0.67 and 0.46 times) index were significantly decreased by 0.4 and 4 mg/kg 6-PPDQ (Fig. 4). Therefore, repeated 6-PPDQ injection could impair the lung function as characterized by decreased Cchord and Penh index.

3.5. Proteomes analysis of lung tissue of mice after repeated 6-PPDQ injection

Among the mass spectrum, a total of 46,008 peptides were generated. Based on these peptides, 5490 proteins were identified and 5208 proteins were quantified. According to the thresholds of fold change > 2.0 or <0.5, and $p < 0.05$, 38 differentially expressed proteins (DEPs) were screened, including 23 upregulated DEPs and 15 downregulated DEPs (Fig. S2A and Table S1). Volcano plot and heatmap of differentially expressed proteins were shown in Fig. S2B and C, respectively.

Based on the above DEPs, kyoto encyclopedia of genes and genomes (KEGG) pathway analysis and gene ontology (GO) analysis were carried out. Based on the thresholds of $p < 0.05$ by fisher's exact test, KEGG pathway analysis showed that 9 enriched pathways (Fig. 5A and Table S2). Based on the thresholds of $p < 0.05$ by fisher's exact test, GO analysis showed that 216, 19, and 53 terms were enriched in biological process (Fig. 5B and Table S3), cellular component (Fig. 5C and Table S4), and molecular function pathways (Fig. 5D and Table S4), respectively.

3.6. The identified differentially expressed proteins associated with 6-PPDQ-induced lung inflammation

Among DEPs screened from proteomes analysis, receptor-interacting serine/threonine-protein kinase 1 (Ripk1, FC = 2.07, $p = 0.032$), FAS-associated death domain protein (Fadd, FC =2.80, $p = 0.035$), interleukin-6 receptor subunit beta (Il-6st, FC =3.54, $p = 0.024$), and pro-interleukin-16 (Il-16, FC = 2.64, $p = 0.0087$) are inflammation related in lung. Expressions of these 4 proteins were increased by 6-

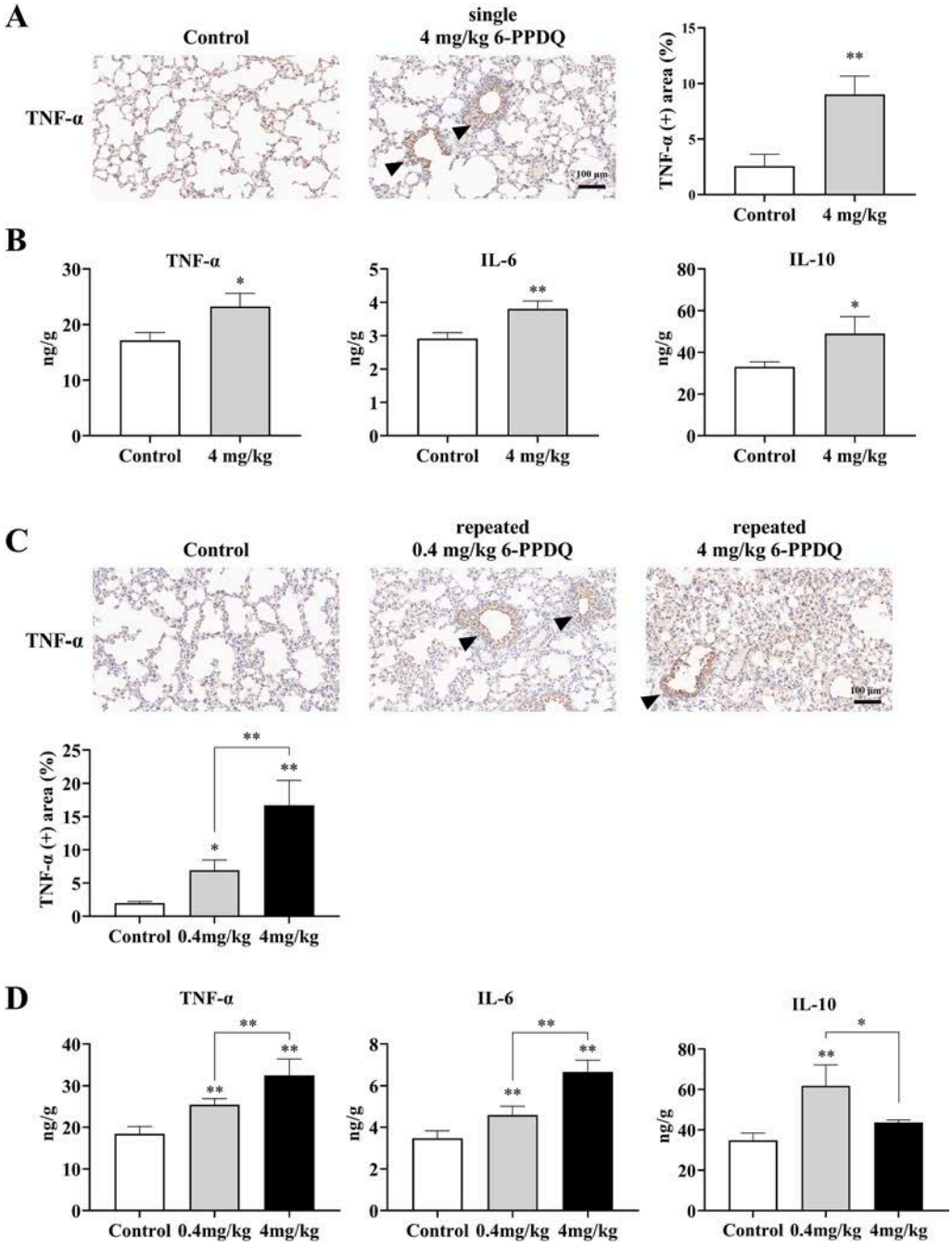

Fig. 2. Effects of 6-PPDQ on cytokine production in lung after single and repeated 6-PPDQ injection. (A) TNF-α immunohistochemistry staining results after single 4 mg/kg 6-PPDQ injection. Arrow heads indicated protein accumulation with high expression. TNF-α positive area in views was analyzed. (B) Levels of TNF-α, IL-6, and IL-10 in lung tissue after single 4 mg/kg 6-PPDQ injection. (C) TNF-α immunohistochemistry staining results after repeated 0.4 and 4 mg/kg 6-PPDQ injection. Arrow heads indicated protein accumulation with high expression. TNF-α positive area in views was analyzed. (D) Levels of TNF-α, IL-6, and IL-10 in lung tissue after repeated 0.4 and 4 mg/kg 6-PPDQ injection. $^{*}P < 0.05$, $^{**}P < 0.01$.

PPDQ exposure (Fig. 6A). To verify the DEPs expression determined by proteomes analysis, their transcriptional expressions were measured. Transcriptional analysis showed that repeated injection with 0.4 and 4 mg/kg 6-PPDQ upregulated the mRNA levels of *Ripk1* (1.56 and 2.28 times), *Fadd* (2.64 and 5.21 times), *Il-6st* (2.50 and 3.99 times), and *Il-16* (2.00 and 3.04 times) (Fig. 6B). The transcriptional levels of *Ripk1*, *Fadd*, *Il-6st*, and *Il-16* in 4 mg/kg 6-PPDQ exposed mice were higher than those of 0.4 mg/kg 6-PPDQ exposed mice (Fig. 6B). Moreover, we measured the protein level of p-Ripk1 and Ripk1 by immunohistochemical staining, and the results showed that repeated injection with 0.4 and 4 mg/kg 6-PPDQ significantly increased p-Ripk1 level (2.42 and 3.24 times) and Ripk1 level (1.57 and 2.00 times) in lung tissue (Fig. 6C). In addition, the expression level of p-Ripk1 (1.34 times) in lung tissue of 4 mg/kg 6-PPDQ exposed mice was also higher than that of 0.4 mg/kg 6-PPDQ exposed mice (Fig. 6C). Moreover, p-Ripk1/Ripk1 ratio was significantly upregulated (1.45 and 1.66 times) by 0.4 and 4 mg/kg 6-PPDQ (Fig. 6C).

In the view of function analysis, Ripk1 and Fadd were included in amounts of inflammation-related enriched terms, such as cytosolic DNA-sensing pathway in KEGG analysis, necroptotic signaling pathway, positive regulation of macrophage differentiation, and regulation of necrotic cell death in biological process of GO analysis. In addition, Il-6st

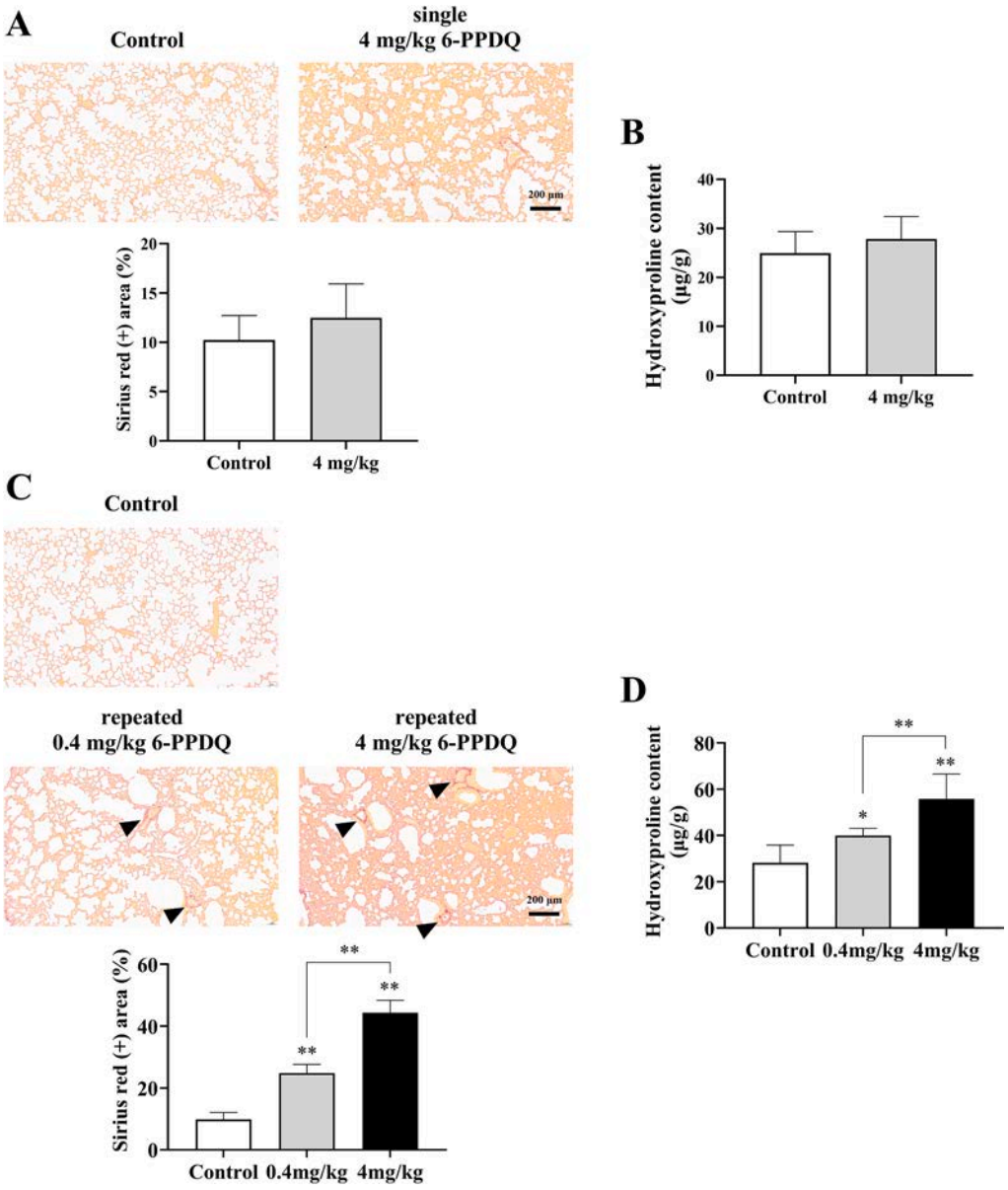

Fig. 3. Effects of 6-PPDQ on fibrosis in lung after single and repeated 6-PPDQ injection. Sirius red staining results (A) and hydroxyproline content (B) after single 4 mg/kg 6-PPDQ injection. Sirius red staining results (C) and hydroxyproline content (D) after repeated 0.4 and 4 mg/kg 6-PPDQ injection. Sirius red positive area in views was analyzed. Arrowheads indicate in the areas with higher level of staining. $^{*}P < 0.05$, $^{**}P < 0.01$.

was included in inflammation-related enriched terms, including cytokine-cytokine receptor interaction, and viral protein interaction with cytokine and cytokine receptor in KEGG analysis, interleukin-11-mediated signaling pathway, interleukin-27-mediated signaling pathway, cytokine-mediated signaling pathway, and cellular response to interleukin-6 in biological process of GO analysis. Il-16 was also included in inflammation-related enriched terms, such as cytokine-cytokine receptor interaction in KEGG analysis, cytokine-mediated signaling pathway, regulation of interleukin-1 alpha production, and regulation of interleukin-12 secretion in biological process of GO analysis.

3.7. The identified differentially expressed protein associated with 6-PPDQ-induced lung fibrosis

Among DEPs screened from proteomes analysis, SMAD family member 2 (Smad2, FC = 2.77, $p = 0.028$) is fibrosis related in lung, and its expression was increased by 6-PPDQ exposure (Fig. 7A). Transcriptional analysis confirmed the increase in *Smad2* expression (2.24 and 3.41 times) by repeated injection with 0.4 and 4 mg/kg 6-PPDQ (Fig. 7B). Besides this, immunohistochemical stain of p-Smad2 showed that repeated injection with 0.4 and 4 mg/kg 6-PPDQ significantly increased p-Smad2 level (3.10 and 6.76 times) and Smad2 level (2.33 and 4.07 times) in lung tissue (Fig. 7C). In addition, both transcriptional expression of *Smad2* and protein expression of Smad2 in 4 mg/kg 6-PPDQ exposed mice was higher than those in 0.4 mg/kg 6-PPDQ exposed mice (Fig. 7C). More importantly, p-Smad2/Smad2 ratio was significantly upregulated (1.36 and 1.78 times) by 0.4 and 4 mg/kg 6-PPDQ (Fig. 7C).

As for function analysis, Smad2 was included in fibrosis-related enriched terms, such as heteromeric SMAD protein complex in cellular component of GO analysis, co-SMAD binding, and transforming growth factor beta receptor, cytoplasmic mediator activity in molecular function of GO analysis.

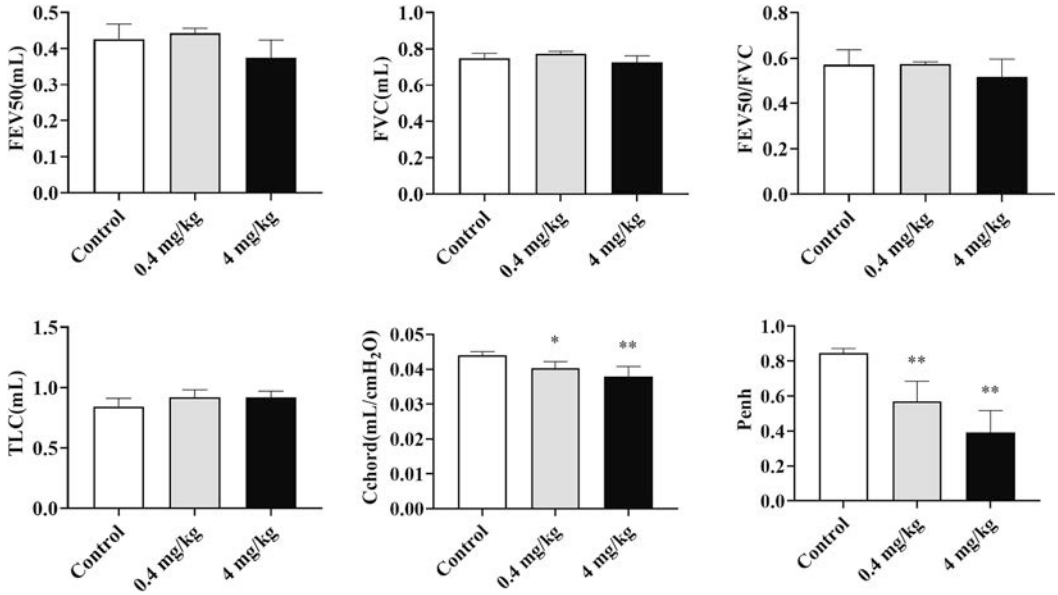

Fig. 4. Effects of 6-PPDQ on lung function after repeated 6-PPDQ injection. Forced vital capacity (FVC), FEV50/FVC, total lung capacity (TLC), chord compliance (Cchord), and enhanced pause (Penh) were measured by plethysmograph system CRFM100. $^{*}P < 0.05$, $^{**}P < 0.01$.

4. Discussion

6-PPDQ is one highly toxic pollutant in TRWP, whose environmental occurrence was first verified in aquatic environment, and poses huge threat to aquatic animals (Tian et al., 2021). Increasing evidence has showed that 6-PPDQ can be detected in various environmental media, even in daily food and human urine (Du et al., 2022; Ji et al., 2022b). In environmental media, the 6-PPDQ ranges from ng/L to μg/L (Tian et al., 2021; Zhang et al., 2022). Due to high sensitivity to different environmental pollutants (Hua et al., 2023d; Shao et al., 2023; Wang et al., 2023b; Liu et al., 2024), *Caenorhabditis elegans* was recently used as animal model to evaluate toxicity of 6-PPDQ at environmentally relevant concentrations. In *C. elegans*, 6-PPDQ at concentrations of 1 and 10 μg/L could cause intestinal toxicity, reproductive toxicity, neurotoxicity, reductio in lifespan, enhancement in lipid accumulation, and dysfunction in dopamine metabolism (Hua et al., 2023a, 2023b, 2023c; Hua and Wang, 2023a; Hua and Wang, 2023b; Wang et al., 2023a). However, 6-PPDQ toxicity to mammals and human beings was not fully understood. Our pervious study demonstrated that 6-PPDQ induced damage to multiple organs, especially liver and lung, in mice (He et al., 2023). The detailed damage on liver and underlying molecular basis were described recently in mice (Fang et al., 2023). In this study, we further focused on the examination of 6-PPDQ damage on lung and underlying molecular basis in mice.

In consideration of high level of 6-PPDQ accumulation in lung (He et al., 2023), we investigated the effects of two different exposure modes, single or repeated injections, on 6-PPDQ bioaccumulation in mouse lung. The 6-PPDQ in the peritoneum can be delivered into mesenteric vessels, then enter the systemic circulation after passing the portal vein and liver, finally accumulate in the lung (Lukas et al., 1971). There are multiple families of xenobiotica-metabolizing enzymes in lung, including cytochromes P450 (CYP), non-CYP oxidoreductases, hydrolases, and conjugating enzymes, which may contribute to the metabolism and detoxification of 6-PPDQ in mouse lung (Oesch et al., 2019). After single injection of 4 mg/kg 6-PPDQ at day 0, rapid decline of 6-PPDQ level was observed in the first 7 days (Fig. 1A). After that, certain level of 6-PPDQ remained in lung tissue up to day 28 (Fig. 1A). Lipid-soluble substances cross alveolo-capillary faster than water-soluble substances (Nilsson and Wollmer, 1993). Thus, it was speculated that 6-PPDQ in blood could be transferred, and accumulated in lung tissue for a long time. Moreover, after repeated injection, lung 6-PPDQ level of 4 mg/kg 6-PPDQ exposure was much higher than that of single injection at day 28 (Fig. 1), which suggested the possible more severe toxicity after repeated 6-PPDQ injection than single 6-PPDQ injection. As showed in Fig. 1A, 6-PPDQ level decreased ~62 % four days post single injection compared to that of one day post injection, therefore, it was speculated that the part of 6-PPDQ injected four days before sacrifice still retained in lung for mice receiving repeated 0.4 mg/kg 6-PPDQ, which caused almost similar level of lung 6-PPDQ was detected between single injection with 4 mg/kg 6-PPDQ, and repeated injection with 0.4 mg/kg 6-PPDQ (Fig. 1).

For the 6-PPDQ-induced toxicity, both single and repeated 6-PPDQ injection could induce obvious inflammation, as verified by alterations in multiple cytokines (TNF-α, IL-6, and IL-10) production in lung (Fig. 2). In response to environmental stimuli, lung can activate the inflammation to overcome the harmful stimulation and initiate repair process (Wong et al., 2016). In our previous study, we found the obvious activation and aggregation of alveolar macrophages in mouse lung after 6-PPDQ injection, as determined by F4/80 immunohistochemical stain (He et al., 2023). Alveolar macrophage can be the first cell type to contact irritants by migrating to the injured or infected lung tissue, and the cytokines produced by various cell populations can initiate and expand local and even systemic immune response via cytokine networks (Borthwick et al., 2013; Wong et al., 2016). The pro-inflammatory cytokines IL-6 and TNF-α are proved to act as key cytokines to promote inflammation (Oikonomou et al., 2006; Stancil et al., 2022), which were significantly increased in lung of 6-PPDQ injected mice as verified by ELISA and immunohistochemistry analysis (Fig. 2). Immunohistochemistry stain can label the intracellular cytokine proteins, but not secreted cytokine proteins outside the cell. On the contrary, ELISA can detect cytokine proteins both inside and outside the cell (Bienvenu et al., 1998; Turlej, 2009). TNF-α protein can both stay inside the cell, and secrete outside the cell (Black et al., 1997). Therefore, different label range resulted in the different fold change in TNF-α protein between two methods (Fig. 2). Importantly, our proteomes analysis showed that cytokine-related proteins (Il-6st and Il-16) were also obviously upregulated by 6-PDDQ (Fig. 6A). We also observed the increases in serum TNF-α and IL-6 levels after 6-PPDQ exposure (Fig. S1B and C), indicating that 6-PPDQ induced the inflammatory response in not only local lung but also systemic range. After repeated injection, 4 mg/kg 6-PPDQ induced

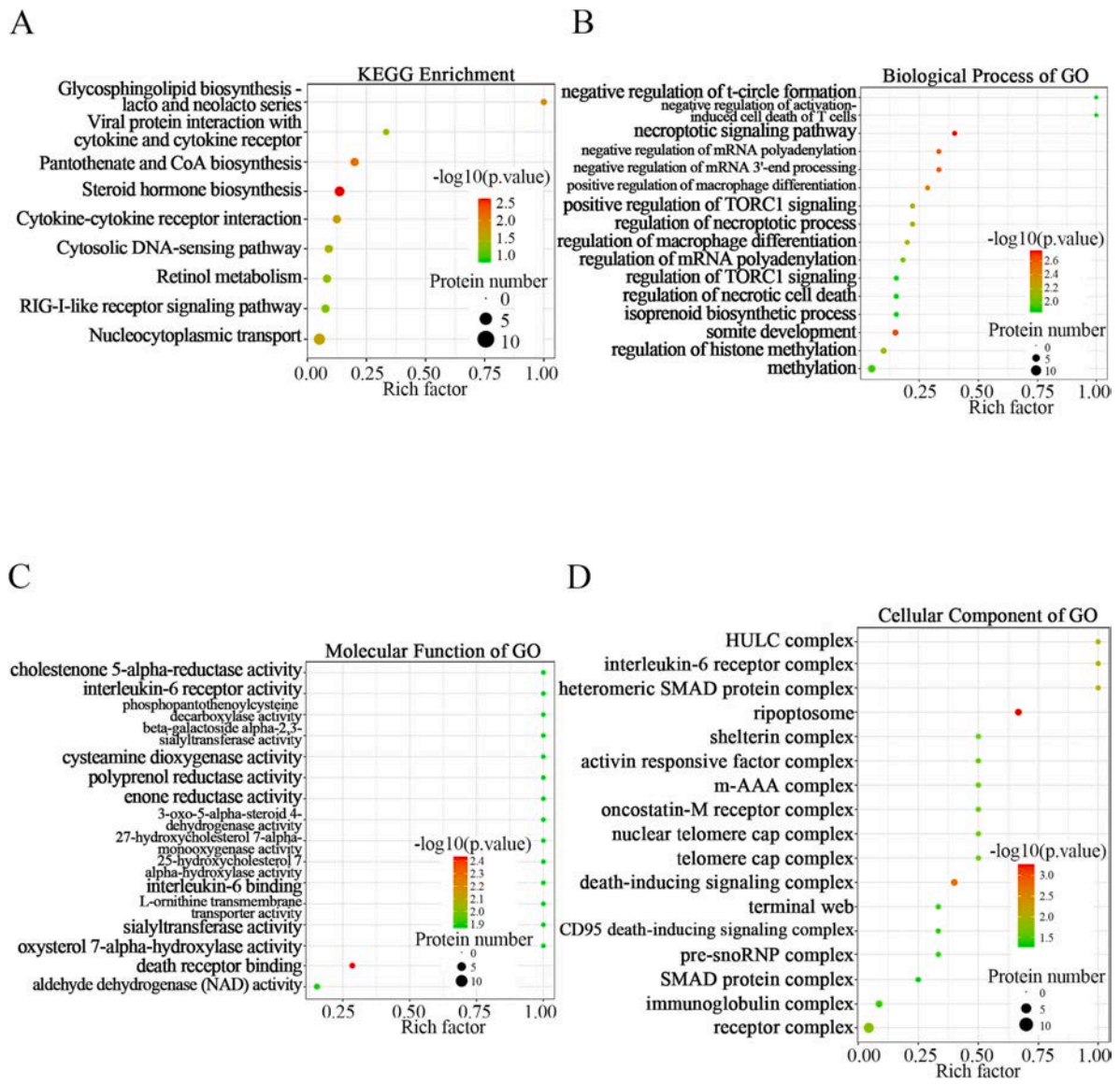

Fig. 5. Bioinformatical analysis of differentially expression proteins caused by repeated 6-PPDQ injection. (A) Top 20 terms of Kyoto Encyclopedia of Genes and Genomes (KEGG) pathway analysis. (B–D) Top 20 terms of biological process, molecular function, and cellular component of Gene Ontology (GO) analysis.

the higher production of pro-inflammatory cytokines (TNF-α and IL-6) than 0.4 mg/kg 6-PPDQ, which was attributed to higher 6-PPDQ accumulation in serum (Fig. S1A and C). Meanwhile, IL-10 level can keep normal or decrease in patients with lung fibrosis (Freeburn et al., 2005; Martinez et al., 1997). IL-10 level in lung and serum of repeated injection with 4 mg/kg 6-PPDQ was significantly lower than that of 0.4 mg/kg 6-PPDQ, and consistent with control (Fig. 2D and S1). This suggested that, after 0.4 mg/kg 6-PPDQ injection, the IL-10 acting as anti-inflammatory cytokine could be activated to be against the inflammation in lung and serum. However, after 4 mg/kg 6-PPDQ injection, this tendency driven by IL-10 was suppressed in lung. Also, 6-PPDQ oral administration caused inflammatory response by promoting production of several cytokines in mouse liver (Fang et al., 2023).

Besides induction of inflammation, repeated 6-PPDQ injection could cause the lung fibrosis. Fibrosis means that an excessive amount of fibrillar extracellular matrix (ECM) proteins, and the collagen is an important family of ECM proteins (Dewidar et al., 2019). Sirius red staining reflected the increased collagen content in lung of mice with repeated 6-PPDQ injection rather than single 6-PPDQ injection (Fig. 3). Hydroxyproline is one of the most abundant amino acids in protein collagen, which is a vital biomarker in fibrosis diagnosis (Gabr et al., 2017). Hydroxyproline content was significantly elevated by repeated 6-PPDQ injection rather than single 6-PPDQ injection (Fig. 3). Therefore, repeated 6-PPDQ injection for four weeks not only initiated chronic inflammation, but also caused fibrosis in mouse lung. Different from this, single 6-PPDQ injection induced lung inflammation but not the fibrosis. Pro-inflammatory cytokines IL-6 and TNF-α also function to regulate fibrosis of lung (Oikonomou et al., 2006; Stancil et al., 2022). More importantly, chronic inflammation can induce fibrosis development by accumulation of extra cellular matrix (ECM). Thus, fibrosis is often accompanied by local inflammation in tissues (Borthwick et al., 2013).

The evidence has showed that lung microstructural changes contribute to the impairment of lung functions (Subramaniam et al., 2017). Our recent study has shown that repeated 6-PPDQ injection induced damage to some aspects of lung structures, such as increased lung index, swollen alveolar capillaries, and exudation in lung interstitium (He et al., 2023). We here further observed obvious inflammation and fibrosis in lung after repeated 6-PPDQ injection (Figs. 2 and 3). The decreased compliance happened in many pathological states, such as alveolar exudation, inflammation, and fibrosis (Özdilek, 2022), which all appeared in lung of 6-PPDQ injected mice. Among the lung functions

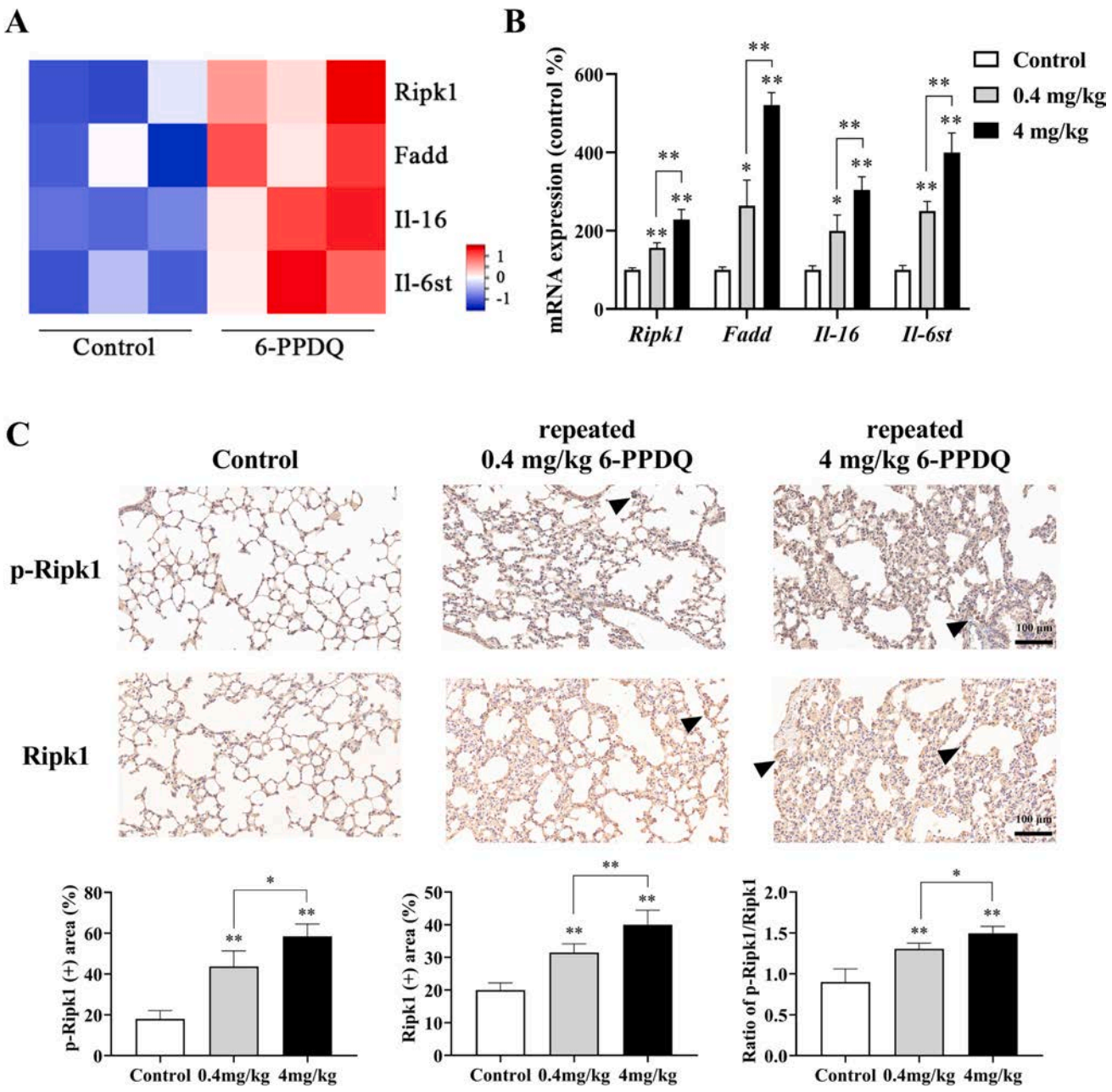

Fig. 6. Screen of inflammation-associated proteins changed by repeated 6-PPDQ injection. (A) Heatmap of inflammation-associated proteins in proteomes analysis. (B) Verification of transcription levels of inflammation-associated genes in 6-PPDQ exposed mice. (C) Representative images of p-Ripk1 and Ripk1 immunohistochemistry staining after repeated 0.4 and 4 mg/kg 6-PPDQ injection. Arrow heads indicated protein accumulation with high expression. The p-Ripk and Ripk1 positive area in views was analyzed. The ratio of p-Ripk1 positive percentage to Ripk1 positive percentage was analyzed. $^{*}P < 0.05$, $^{**}P < 0.01$.

detected by plethysmograph system, Cchord and Penh were significantly downregulated by repeated 6-PPDQ injection (Fig. 4). Lung compliance is defined as the volume change per unit change in pressure gradient, and Cchord can reflect the elastic resistance of the lung (Özdilek, 2022). Enhanced pause (Penh) was used as an indicator of airway responsiveness (Lomask, 2006), and airway responsiveness is a well-established characteristic of asthma (Archer et al., 2004). Thus, it was speculated that 6-PPDQ might have the potential to act as allergen to impair lung function. Notably, as the 6-PPDQ former, 6-PPD was also regarded as allergen for tyre-induced occupational eczema (Herve-Bazin et al., 1977). Given to high detection rate of 6-PPDQ in $PM_{2.5}$ (Zhang et al., 2022), potential association between 6-PPDQ inhalation and asthma or allergy in population should be noticed. Collectively, 6-PPDQ injection can disturbed elastic resistance and airway responsiveness of mouse lung, and may in turn impair the lung function.

Ripoptosome containing receptor-interacting serine/threonine-protein kinase 1 (Ripk1), FAS-associated death domain protein (Fadd), and Caspase-8 regulate cell death type between necroptosis and apoptosis in response to different stress conditions (Bertrand and Vandenabeele, 2011). Proteomics analysis indicated that expressions of Ripk1 and Fadd were both significantly increased (Fig. 6A). Transcriptional assay and immunohistochemistry staining verified that mRNA levels of *Ripk1* and *Fadd*, phosphorylation level of Ripk1, and ratio of p-Ripk1/Ripk1 were significantly increased after repeated 6-PPDQ injection (Fig. 6B and C). Under the condition of TNF-α stimulation, necrosome complex consisted of Ripk1, and Ripk3 activated the mixed lineage kinase-like protein (Mlkl), which then causes rapid plasma membrane lysis to induce cell death called necroptosis (Degterev et al., 2019). Ripk1 can also mediate

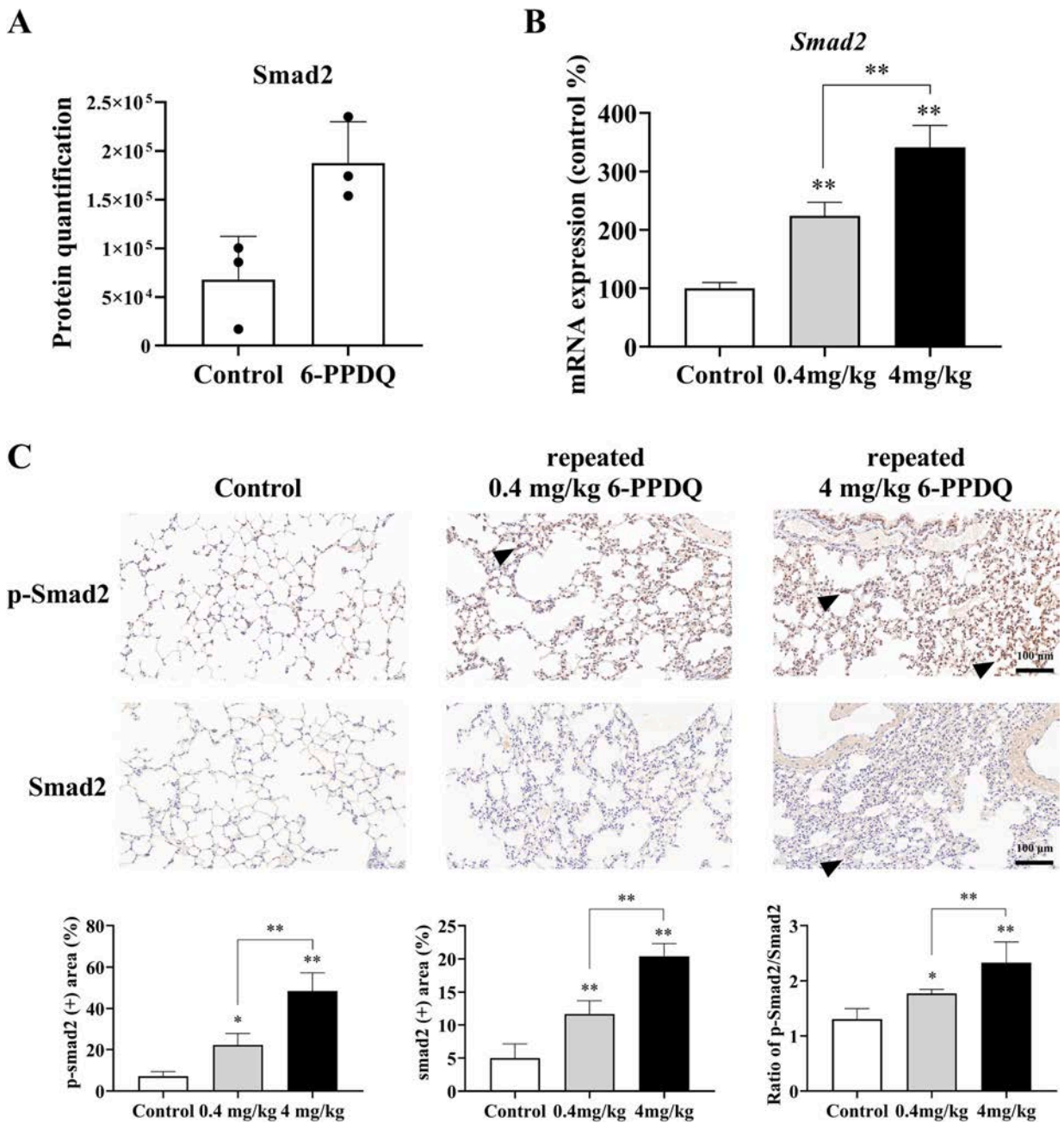

Fig. 7. Screen of fibrosis-associated proteins changed by repeated 6-PPDQ injection. (A) Protein quantification of Smad2 in proteomes analysis. (B) Verification of transcription level of *Smad2* in 6-PPDQ exposed mice. (C) Representative images of p-Smad2 and Smad2 immunohistochemistry staining after repeated 0.4 and 4 mg/kg 6-PPDQ injection. Arrow heads indicated protein accumulation with high expression. The p-Smad2 positive area in views was analyzed. The ratio of p-Smad2 positive percentage to Smad2 positive percentage was analyzed. $^{*}P < 0.05$, $^{**}P < 0.01$.

inflammatory gene expression independence of damage-associated molecular patterns (DAMPs) (Degterev et al., 2019). As for ripoptosome, absence of Caspase-8 can start Ripk1-dependent necroptosis rather than apoptosis (Newton, 2015). Nevertheless, based on proteomics analysis, Caspase-8 expression was not significantly changed (Table S1). Thus, necroptosis but not apoptosis might happen in mouse lung with 6-PPDQ injection. Meanwhile, numerous terms (TNF signaling pathway, necroptotic signaling pathway, and regulation of necroptotic process) associated with necroptosis were enriched in enrichment of KEGG pathway and GO analysis (Fig. 5).

Cytokine production occurs in necroptosis-induced inflammatory response (Yan et al., 2022). Notably, the cytokine plays a key role in mediating immune response and fibrosis process (Borthwick et al., 2013). In proteomic analysis, cytokines-related proteins, pro-interleukin-16 (Il-16) and interleukin-6 receptor subunit beta (Il-6st), were significantly upregulated (Fig. 6A). Meanwhile, mRNA levels of *Il-16* and *Il-6st* were also obviously upregulated by 6-PPDQ (Fig. 6B). Il-16 was initially regarded as T cell chemoattractant, and functions by recruitment and activation of CD4+ cells in several autoimmune diseases (Cruikshank et al., 2000). Il-16 could trigger inflammatory response via neutrophil recruitment, eosinophil chemoattractant, and cytokines production by Th2 and Th17 in lung diseases (Bowler et al., 2013; Cheng et al., 2001; Li et al., 2019; Smith et al., 2018). Interleukin-6 receptor subunit beta (Il-6st), also named glycoprotein 130 (gp130), binds to complex of Il6 and interleukin-6 receptor (l6-R) to initiate intracellular signaling (Rose-John, 2012). Il-6st increase was found in

multiple lung diseases with inflammation, such as acute lung injury, and chronic lung disease (Chakraborty et al., 2013; Xu et al., 2023). Therefore, both Il-16 and Il-6st further functioned to mediate cytokine signaling, and then contributed to the inflammatory response in lung.

Smad2 is a key component for transforming growth factor-β (TGF-β) signaling pathway, the master regulator of fibrosis (Meng et al., 2016). In TGF-β signaling pathway, Smads are phosphorylated and transferred into the nucleus to start transcription of fibrosis-related genes (Kisseleva and Brenner, 2021; Meng et al., 2016). Smad2 plays a key role in controlling tissue fibrosis (Gregory et al., 2010; Khalil et al., 2017). Our proteomics analysis showed that Smad2 was significantly upregulated by repeated 6-PPDQ injection (Fig. 7A). The *Smad2* mRNA was increased by 6-PPDQ (Fig. 7B). Immunohistochemistry staining further showed that the phosphorylated Smad2 level and p-Smad2/Smad2 ratio was markedly promoted in lung tissue (Fig. 7C). Besides the role of Smad2 in 6-PPDQ-induced lung fibrosis, Ripk1and cytokines of Il-16 and Il-6st may also play important roles. Ripk1 activation could be observed in fibrosis state of multiple tissue (Mou and Mou, 2020; Srivastava et al., 2022; Tan et al., 2020). Il-16 could induce macrophage infiltration and cardiac fibrosis in hypertensive mice (Tamaki et al., 2013). Il-6st was also proved to participate in tissue fibrosis (Mozaffarian et al., 2008; Tang et al., 2017; Tao et al., 2014). Therefore, repeated 6-PPDQ injection caused lung fibrosis by activating multiple molecular signals, including Smad2, Ripk1, and cytokines of Il-16 and Il-6st.

5. Conclusions

In mice model, we examined the 6-PPDQ dynamic bioaccumulation, toxicity in causing inflammation and fibrosis, and the underlying molecular basis by proteomes analysis. 6-PPDQ remained in lung tissue up to day 28 after single injection, and high level of 6-PPDQ was detected in lung of repeated injection mice. Both severe inflammation and fibrosis were detected in lung after repeated 6-PPDQ injection. Repeated 6-PPDQ injection also severely impaired lung function, as verified by decreased Cchord and Penh index. Moreover, the proteomes analysis identified differently expressed proteins associated with 6-PPDQ-induced inflammation (Ripk1, Fadd, Il-6st, and Il-16) and fibrosis (Smad2). Our results highlight the potential of long-term exposure to 6-PPDQ in causing damage on lung by inducing inflammation and fibrosis in mammals.

CRediT authorship contribution statement

Wenmiao He: Writing – original draft, Investigation. **Jie Chao:** Methodology. **Aihua Gu:** Supervision. **Dayong Wang:** Writing – review & editing, Supervision.

Declaration of competing interest

The authors declare that they have no known competing financial interests or personal relationships that could have appeared to influence the work reported in this paper.

Appendix A. Supplementary data

Supplementary data to this article can be found online at https://doi.org/10.1016/j.scitotenv.2024.171220.

References

Archer, A.J., Cramton, J.L., Pfau, J.C., Colasurdo, G., Holian, A., 2004. Airway responsiveness after acute exposure to urban particulate matter 1648 in a DO11.10 murine model. Am. J. Phys. Lung Cell. Mol. Phys. 286, L337–L343.

Bertrand, M.J., Vandenabeele, P., 2011. The Ripoptosome: death decision in the cytosol. Mol. Cell 43, 323–325.

Bienvenu, J.A., Monneret, G., Gutowski, M.C., Fabien, N., 1998. Cytokine assays in human sera and tissues. Toxicology 129, 55–61.

Black, R.A., Rauch, C.T., Kozlosky, C.J., Peschon, J.J., Slack, J.L., Wolfson, M.F., Castner, B.J., Stocking, K.L., Reddy, P., Srinivasan, S., Nelson, N., Boiani, N., Schooley, K.A., Gerhart, M., Davis, R., Fitzner, J.N., Johnson, R.S., Paxton, R.J., March, C.J., Cerretti, D.P., 1997. A metalloproteinase disintegrin that releases tumour-necrosis factor-alpha from cells. Nature 385, 729–733.

Borthwick, L.A., Wynn, T.A., Fisher, A.J., 2013. Cytokine mediated tissue fibrosis. Biochim. Biophys. Acta 1832, 1049–1060.

Bowler, R.P., Bahr, T.M., Hughes, G., Lutz, S., Kim, Y.I., Coldren, C.D., Reisdorph, N., Kechris, K.J., 2013. Integrative omics approach identifies interleukin-16 as a biomarker of emphysema. OMICS 17, 619–626.

Chakraborty, M., McGreal, E.P., Davies, P.L., Nowell, M.A., Jones, S., Kotecha, S., 2013. Role of interleukin-6, its receptor and soluble gp130 in chronic lung disease of prematurity. Neonatology 104, 161–167.

Cheng, G., Ueda, T., Eda, F., Arima, M., Yoshida, N., Fukuda, T., 2001. A549 cells can express interleukin-16 and stimulate eosinophil chemotaxis. Am. J. Respir. Cell Mol. Biol. 25, 212–218.

Cruikshank, W.W., Kornfeld, H., Center, D.M., 2000. Interleukin-16. J. Leukoc. Biol. 67, 757–766.

Degterev, A., Ofengeim, D., Yuan, J., 2019. Targeting RIPK1 for the treatment of human diseases. Proc. Natl. Acad. Sci. USA 116, 9714–9722.

Deng, C., Huang, J., Qi, Y., Chen, D., Huang, W., 2022. Distribution patterns of rubber tire-related chemicals with particle size in road and indoor parking lot dust. Sci. Total Environ. 844, 157144.

Dewidar, B., Meyer, C., Dooley, S., Meindl-Beinker, A.N., 2019. TGF-β in hepatic stellate cell activation and liver fibrogenesis-updated 2019. Cells 8.

Du, B., Liang, B., Li, Y., Shen, M., Liu, L.-Y., Zeng, L., 2022. First report on the occurrence of N-(1,3-dimethylbutyl)-N′-phenyl-p-phenylenediamine (6PPD) and 6PPD-quinone as pervasive pollutants in human urine from South China. Environ. Sci. Technol. Lett. 9, 1056–1062.

Fang, L., Fang, C., Di, S., Yu, Y., Wang, C., Wang, X., Jin, Y., 2023. Oral exposure to tire rubber-derived contaminant 6PPD and 6PPD-quinone induce hepatotoxicity in mice. Sci. Total Environ. 869, 161836.

Foth, H., 1995. Role of the lung in accumulation and metabolism of xenobiotic compounds—implications for chemically induced toxicity. Crit. Rev. Toxicol. 25, 165–205.

Freeburn, R.W., Armstrong, L., Millar, A.B., 2005. Cultured alveolar macrophages from patients with idiopathic pulmonary fibrosis (IPF) show dysregulation of lipopolysaccharide-induced tumor necrosis factor-alpha (TNF-alpha) and interleukin-10 (IL-10) inductions. Eur. Cytokine Netw. 16, 5–16.

Gabr, S.A., Alghadir, A.H., Sherif, Y.E., Ghfar, A.A., 2017. Hydroxyproline as a biomarker in liver disease. In: Patel, V.B., Preedy, V.R. (Eds.), Biomarkers in Liver Disease. Springer, Netherlands, Dordrecht, pp. 471–491.

Gregory, L.G., Mathie, S.A., Walker, S.A., Pegorier, S., Jones, C.P., Lloyd, C.M., 2010. Overexpression of Smad2 drives house dust mite-mediated airway remodeling and airway hyperresponsiveness via activin and IL-25. Am. J. Respir. Crit. Care Med. 182, 143–154.

He, W., Gu, A., Wang, D., 2023. Four-week repeated exposure to tire-derived 6-PPD quinone causes multiple organ injury in male BALB/c mice. Sci. Total Environ. 894, 164842.

Herve-Bazin, B., Gradiski, D., Duprat, P., Marignac, B., Foussereau, J., Cavelier, C., Bieber, P., 1977. Occupational eczema from N-isopropyl -N'-phenylparaphenylenediamine (IPPD) and N-dimethy-1,3 butyl-N'-phenylparaphenylenediamine (DMPPD) in tyres. Contact Derm. 3, 1–15.

Hiki, K., Yamamoto, H., 2022. The tire-derived chemical 6PPD-quinone is lethally toxic to the white-spotted char *Salvelinus leucomaenis* pluvius but not to two other salmonid species. Environ. Sci. Technol. Lett. 9, 1050–1055.

Hua, X., Wang, D., 2023a. Disruption of dopamine metabolism by exposure to 6-PPD quinone in *Caenorhabditis elegans*. Environ. Pollut. 337, 122649.

Hua, X., Wang, D., 2023b. Exposure to 6-PPD quinone at environmentally relevant concentrations inhibits both lifespan and healthspan in *C. elegans*. Environ. Sci. Technol. 57, 19295–19303.

Hua, X., Feng, X., Liang, G., Chao, J., Wang, D., 2023a. Long-term exposure to tire-derived 6-PPD quinone causes intestinal toxicity by affecting functional state of intestinal barrier in *Caenorhabditis elegans*. Sci. Total Environ. 861, 160591.

Hua, X., Feng, X., Liang, G., Chao, J., Wang, D., 2023b. Exposure to 6-PPD quinone at environmentally relevant concentrations causes abnormal locomotion behaviors and neurodegeneration in *Caenorhabditis elegans*. Environ. Sci. Technol. 57, 4940–4950.

Hua, X., Feng, X., Liang, G., Chao, J., Wang, D., 2023c. Long-term exposure to 6-PPD quinone reduces reproductive capacity by enhancing germline apoptosis associated with activation of both DNA damage and cell corpse engulfment in *Caenorhabditis elegans*. J. Hazard. Mater. 454, 131495.

Hua, X., Cao, C., Zhang, L., Wang, D.-Y., 2023d. Activation of FGF signal in germline mediates transgenerational toxicity of polystyrene nanoparticles at predicted environmental concentrations in *Caenorhabditis elegans*. J. Hazard. Mater. 451, 131174.

Islam, M.S., Larpruenrudee, P., Saha, S.C., Pourmehran, O., Paul, A.R., Gemci, T., Collins, R., Paul, G., Gu, Y., 2021. How severe acute respiratory syndrome coronavirus-2 aerosol propagates through the age-specific upper airways. Phys. Fluids (1994) 33, 081911.

Ji, J., Huang, J., Cao, N., Hao, X., Wu, Y., Ma, Y., An, D., Pang, S., Li, X., 2022a. Multiview behavior and neurotransmitter analysis of zebrafish dyskinesia induced by 6PPD and its metabolites. Sci. Total Environ. 838, 156013.

Ji, J., Li, C., Zhang, B., Wu, W., Wang, J., Zhu, J., Liu, D., Gao, R., Ma, Y., Pang, S., Li, X., 2022b. Exploration of emerging environmental pollutants 6PPD and 6PPDQ in honey and fish samples. Food Chem. 396, 133640.

Khalil, H., Kanisicak, O., Prasad, V., Correll, R.N., Fu, X., Schips, T., Vagnozzi, R.J., Liu, R., Huynh, T., Lee, S.J., Karch, J., Molkentin, J.D., 2017. Fibroblast-specific TGF-β-Smad2/3 signaling underlies cardiac fibrosis. J. Clin. Invest. 127, 3770–3783.
Kisseleva, T., Brenner, D., 2021. Molecular and cellular mechanisms of liver fibrosis and its regression. Nat. Rev. Gastroenterol. Hepatol. 18, 151–166.
Li, C., Dai, J., Dong, G., Ma, Q., Li, Z., Zhang, H., Yan, F., Zhang, J., Wang, B., Shi, H., Zhu, Y., Yao, X., Si, C., Xiong, H., 2019. Interleukin-16 aggravates ovalbumin-induced allergic inflammation by enhancing Th2 and Th17 cytokine production in a mouse model. Immunology 157, 257–267.
Liu, Y., Chen, H., Wu, S., Gao, J., Li, Y., An, Z., Mao, B., Tu, R., Li, T., 2022. Impact of vehicle type, tyre feature and driving behaviour on tyre wear under real-world driving conditions. Sci. Total Environ. 842, 156950.
Liu, Z.-Y., Hua, X., Zhao, Y., Bian, Q., Wang, D.-Y., 2024. Polyethylene nanoplastics cause reproductive toxicity associated with activation of both estrogenic hormone receptor NHR-14 and DNA damage checkpoints in *C. elegans*. Sci. Total Environ. 906, 167471.
Lomask, M., 2006. Further exploration of the Penh parameter. Exp. Toxicol. Pathol. 57 (Suppl. 2), 13–20.
Lukas, G., Brindle, S.D., Greengard, P., 1971. The route of absorption of intraperitoneally administered compounds. J. Pharmacol. Exp. Ther. 178, 562–564.
Martinez, J.A., King Jr., T.E., Brown, K., Jennings, C.A., Borish, L., Mortenson, R.L., Khan, T.Z., Bost, T.W., Riches, D.W., 1997. Increased expression of the interleukin-10 gene by alveolar macrophages in interstitial lung disease. Am. J. Phys. 273 (L676-683).
Meng, X.M., Nikolic-Paterson, D.J., Lan, H.Y., 2016. TGF-β: the master regulator of fibrosis. Nat. Rev. Nephrol. 12, 325–338.
Mou, F., Mou, C., 2020. Necrostatin-1 alleviates bleomycin-induced pulmonary fibrosis and extracellular matrix expression in interstitial pulmonary fibrosis. Med. Sci. Monit. 26, e919739.
Mozaffarian, A., Brewer, A.W., Trueblood, E.S., Luzina, I.G., Todd, N.W., Atamas, S.P., Arnett, H.A., 2008. Mechanisms of oncostatin M-induced pulmonary inflammation and fibrosis. J. Immunol. 181, 7243–7253.
Newton, K., 2015. RIPK1 and RIPK3: critical regulators of inflammation and cell death. Trends Cell Biol. 25, 347–353.
Nilsson, K., Wollmer, P., 1993. Pulmonary clearance of tracers with different lipid and water solubility in experimental surfactant dysfunction. Eur. Respir. J. 6, 505–508.
Oesch, F., Fabian, E., Landsiedel, R., 2019. Xenobiotica-metabolizing enzymes in the lung of experimental animals, man and in human lung models. Arch. Toxicol. 93, 3419–3489.
Oikonomou, N., Harokopos, V., Zalevsky, J., Valavanis, C., Kotanidou, A., Szymkowski, D.E., Kollias, G., Aidinis, V., 2006. Soluble TNF mediates the transition from pulmonary inflammation to fibrosis. PLoS One 1, e108.
Özdilek, A., 2022. Lung mechanics-compliance and resistance-extrapulmonary response. In: Esquinas, A.M. (Ed.), Teaching Pearls in Noninvasive Mechanical Ventilation: Key Practical Insights. Springer International Publishing, Cham, pp. 103–109.
Rose-John, S., 2012. IL-6 trans-signaling via the soluble IL-6 receptor: importance for the pro-inflammatory activities of IL-6. Int. J. Biol. Sci. 8, 1237–1247.
Seiwert, B., Nihemaiti, M., Troussier, M., Weyrauch, S., Reemtsma, T., 2022. Abiotic oxidative transformation of 6-PPD and 6-PPD quinone from tires and occurrence of their products in snow from urban roads and in municipal wastewater. Water Res. 212, 118122.
Shao, Y.-T., Wang, Y.-X., Hua, X., Li, Y.-H., Wang, D.-Y., 2023. Polylactic acid microparticles in the range of μg/L reduce reproductive capacity by affecting the gonad development and the germline apoptosis in *Caenorhabditis elegans*. Chemosphere 336, 139193.
Smith, S., Wu, P.W., Seo, J.J., Fernando, T., Jin, M., Contreras, J., Montano, E.N., Gabhann, J.N., Cunningham, K., Widaa, A., McCarthy, E.M., Molloy, E.S., Kearns, G., Murphy, C.C., Kong, W., Björkbacka, H., Kornfeld, H., Forbess, L., Venuturupalli, S., Ishimori, M., Wallace, D., Weisman, M.H., Jefferies, C.A., 2018. IL-16/miR-125a axis controls neutrophil recruitment in pristane-induced lung inflammation. JCI Insight 3.
Srivastava, A., Tomar, B., Sharma, P., Kumari, S., Prakash, S., Rath, S.K., Kulkarni, O.P., Gupta, S.K., Mulay, S.R., 2022. RIPK3-MLKL signaling activates mitochondrial CaMKII and drives intrarenal extracellular matrix production during CKD. Matrix Biol. 112, 72–89.
Stancil, I.T., Michalski, J.E., Hennessy, C.E., Hatakka, K.L., Yang, I.V., Kurche, J.S., Rincon, M., Schwartz, D.A., 2022. Interleukin-6-dependent epithelial fluidization initiates fibrotic lung remodeling. Sci. Transl. Med. 14, eabo5254.
Subramaniam, K., Kumar, H., Tawhai, M.H., 2017. Evidence for age-dependent air-space enlargement contributing to loss of lung tissue elastic recoil pressure and increased shear modulus in older age. J. Appl. Physiol. 1985 (123), 79–87.
Suresh, K., Shimoda, L.A., 2016. Lung circulation. Compr. Physiol. 6, 897–943.
Tamaki, S., Mano, T., Sakata, Y., Ohtani, T., Takeda, Y., Kamimura, D., Omori, Y., Tsukamoto, Y., Ikeya, Y., Kawai, M., Kumanogoh, A., Hagihara, K., Ishii, R., Higashimori, M., Kaneko, M., Hasuwa, H., Miwa, T., Yamamoto, K., Komuro, I., 2013. Interleukin-16 promotes cardiac fibrosis and myocardial stiffening in heart failure with preserved ejection fraction. PLoS One 8, e68893.
Tan, S., Zhao, J., Sun, Z., Cao, S., Niu, K., Zhong, Y., Wang, H., Shi, L., Pan, H., Hu, J., Qian, L., Liu, N., Yuan, J., 2020. Hepatocyte-specific TAK1 deficiency drives RIPK1 kinase-dependent inflammation to promote liver fibrosis and hepatocellular carcinoma. Proc. Natl. Acad. Sci. USA 117, 14231–14242.
Tang, L.Y., Heller, M., Meng, Z., Yu, L.R., Tang, Y., Zhou, M., Zhang, Y.E., 2017. Transforming growth factor-β (TGF-β) directly activates the JAK1-STAT3 axis to induce hepatic fibrosis in coordination with the SMAD pathway. J. Biol. Chem. 292, 4302–4312.
Tao, H., Yang, J.J., Chen, Z.W., Xu, S.S., Zhou, X., Zhan, H.Y., Shi, K.H., 2014. DNMT3A silencing RASSF1A promotes cardiac fibrosis through upregulation of ERK1/2. Toxicology 323, 42–50.
Tian, Z., Zhao, H., Peter, K.T., Gonzalez, M., Wetzel, J., Wu, C., Hu, X., Prat, J., Mudrock, E., Hettinger, R., Cortina, A.E., Biswas, R.G., Kock, F.V.C., Soong, R., Jenne, A., Du, B., Hou, F., He, H., Lundeen, R., Gilbreath, A., Sutton, R., Scholz, N., Davis, J., Dodd, M.C., Simpson, A., McIntyre, J.K., Kolodziej, E.P., 2021. A ubiquitous tire rubber–derived chemical induces acute mortality in coho salmon. Science 371, 185.
Turlej, E., 2009. Novel methods of cytokine detection: real-time PCR, ELISPOT, and intracellular cytokine staining. Postepy Hig. Med. Dosw. (Online) 63, 213–224.
Wang, Y., Hua, X., Wang, D., 2023a. Exposure to 6-PPD quinone enhances lipid accumulation through activating metabolic sensors of SBP-1 and MDT-15 in *Caenorhabditis elegans*. Environ. Pollut. 333, 121937.
Wang, Y.-X., Yuan, X.-A., Zhou, R., Bu, Y.-Q., Wang, D.-Y., 2023b. Combinational exposure to hydroxyatrazine increases neurotoxicity of polystyrene nanoparticles on *Caenorhabditis elegans*. Sci. Total Environ. 880, 163283.
Wiśniewski, J.R., Zougman, A., Nagaraj, N., Mann, M., 2009. Universal sample preparation method for proteome analysis. Nat. Methods 6, 359–362.
Wong, J., Magun, B.E., Wood, L.J., 2016. Lung inflammation caused by inhaled toxicants: a review. Int. J. Chron. Obstruct. Pulmon. Dis. 11, 1391–1401.
Xu, F., Wang, S., Wang, Y., Hu, L., Zhu, L., 2023. Inhibition of gp130 alleviates LPS-induced lung injury by attenuating apoptosis and inflammation through JAK1/STAT3 signaling pathway. Inflamm. Res. 72, 493–507.
Yan, L., Zhang, T., Wang, K., Chen, Z., Yang, Y., Shan, B., Sun, Q., Zhang, M., Zhang, Y., Zhong, Y., Liu, N., Gu, J., Xu, D., 2022. SENP1 prevents steatohepatitis by suppressing RIPK1-driven apoptosis and inflammation. Nat. Commun. 13, 7153.
Zhang, Y., Xu, C., Zhang, W., Qi, Z., Song, Y., Zhu, L., Dong, C., Chen, J., Cai, Z., 2022. p-Phenylenediamine antioxidants in PM(2.5): the underestimated urban air pollutants. Environ. Sci. Technol. 56, 6914–6921.
Zhang, S.Y., Gan, X., Shen, B., Jiang, J., Shen, H., Lei, Y., Liang, Q., Bai, C., Huang, C., Wu, W., Guo, Y., Song, Y., Chen, J., 2023. 6PPD and its metabolite 6PPDQ induce different developmental toxicities and phenotypes in embryonic zebrafish. J. Hazard. Mater. 455, 131601.